Five Regimes of the Quasi-Cnoidal, Steadily Translating Waves of the Rotation-Modified Korteweg-deVries ("Ostrovsky") Equation

John P. Boyd

Department of Atmospheric, Oceanic and Space Science
University of Michigan
2455 Hayward Avenue
Ann Arbor, MI 48109
United States of America
email: jpboyd@engin.umich.edu

Guan-yu Chen

Institute of Harbour and Marine Technology
Wuchi, Taichung 435
Taiwan
email: gychen@mail.ihmt.gov.tw

Abstract

The Rotation-Modified Korteweg-deVries (RMKdV) equation differs from the ordinary KdV equation only through an extra undifferentiated term due to Coriolis force. This article describes the steadily-travelling, spatially-periodic solutions which have peaks of identical size. These generalize the "cnoidal" waves of the KdV equation. There are five overlapping regimes in the parameter space. We derive four different analytical approximations to interpret them. There is also a narrow region where the solution folds over so that there are three distinct shapes at a given point in parameter space. The shortest of these shapes is approximated everywhere in space by a parabola except for a thin interior layer at the crest. A low-order Fourier-Galerkin algorithm, usually thought of as a numerical method, also yields an explicit analytic approximation, too. We illustrate the usefulness of these approximations through comparisons with pseudospectral Fourier numerical computations over the whole parameter space.

Key words: solitary wave, cnoidal wave, water waves

1 Introduction

The Rotation-Modified Korteweg-deVries (RMKdV) equation, which is often called the "Ostrovsky" equation, is a model for gravity waves propagating down a channel under the influence of Coriolis force:

$$\frac{\partial}{\partial x}\left(u_t + uu_x + u_{xxx}\right) - \epsilon^2 u = 0 \qquad \text{RMKdV Eq.} \tag{1}$$

where the non-dimensional parameter $\epsilon \geq 0$ measures the importance of the earth's rotation. In the limit $\epsilon = 0$, this equation reduces to the ordinary Korteweg-deVries equation. The derivation and twenty year history of this equation are discussed at length in [5,8,4,13,12].

The steadily-translating solutions of the RMKdV equation solve the ordinary differential equation

$$-cu_{XX} + u_X^2 + uu_{XX} + u_{4X} - \epsilon^2\, u = 0 \qquad \text{[stationary RMKdV]} \tag{2}$$

where $X = x - ct$ and c is the phase speed. The ODE form of the RMKdV equation, which is henceforth the only problem considered in the rest of the paper, admits a wide variety of solutions including nonlocal solitary waves and spatially-periodic generalizations of nonlocal solitary waves, which have one or more tall, soliton-like peaks plus a number of smaller sinusoidal crests on each spatial period. However, in this article, we concentrate on the simplest solutions: those which have peaks all of the same size, just like the "cnoidal" waves of the KdV equation.

There are at least three motives for being interested in these quasi-cnoidal waves. First, completeness in understanding all the different classes of solutions of the RMKdV equation. Second, complexity in a somewhat surprising place: there are five different regimes for these solutions in spite of their simplicity of shape for any given set of parameters. Third, the more complicated solutions bifurcate from the quasi-cnoidal waves at small but finite ϵ.

Our analysis of the five regimes is greatly simplified by a scaling theorem. The quasi-cnoidal waves depend on three parameters: the phase speed c, the Coriolis parameter ϵ and the spatial period P.[1] The scaling theorem implies that if $v(X; c, \epsilon)$ is a solution, then so also is $u \equiv \lambda^2 v(\lambda X; c\lambda^2, \lambda^2\epsilon)$ for arbitrary constant λ. It follows that there is at most a two-parameter family of distinct shapes, and we can therefore fix one of the parameters without loss

[1] Since the coefficients of the equation are independent of X, $u(X+\Phi)$ is a solution whenever $u(X)$ is a solution for arbitrary constant Φ. However, since this fourth parameter Φ does not alter the *shape* of the wave, we shall henceforth ignore it, and adopt the convention that the crest of the wave is always at $X = 0$.

of generality. Arbitrarily, we adopt Hunter's[14] convention and set $c = 1$ in the rest of this article.

The two shape-determining parameters are then the Coriolis parameter ϵ and the spatial period P. However, it is incovenient to work with P because quasi-cnoidal solutions exist only when $P < P_{max}(\epsilon)$ where P_{max} decreases roughly as $1/\epsilon$. We shall therefore define the "period parameter" ν via

$$\nu \equiv P \frac{\epsilon}{2\pi} \tag{3}$$

In the rest of the article, we derive analytic approximations that describe the quasi-cnoidal waves in various parts of the $\nu - \epsilon$ plane.

2 Overview of the Regime Diagram

Fig. 1 illustrates the five main regimes. The dashes bound a sixth area in parameter space which requires special treatment, as explained below. The large question marks denote the region in parameter space where all four of the analytic approximations derived below fail: this is centered at approximately $\nu \approx 1/2, \epsilon \approx 1/4$. For small ϵ (bottom of the diagram), there is a central peak approximately equal to $3\mathrm{sech}^2(X/2)$ plus a small sinusoidal oscillation which fills the rest of the spatial period; the Hunter-Chen-Boyd matched asymptotics series is a good approximation. Unfortunately, both the description and the approximation fail as $\nu \to 0$ and as $\nu \to 1$.

The right border of the regime diagram, $\nu = \nu_{max}(\epsilon)$ where

$$\nu_{max}(\epsilon) \equiv 2\epsilon/\sqrt{-2 + 2\sqrt{1 + 4\epsilon^2}} \approx 1 + \frac{1}{2}\,\epsilon^2 + O(\epsilon^4), \tag{4}$$

is where the quasi-cnoidal waves are sine waves of infinitesimal amplitude. (This is just the linear dispersion as derived below as Eq. 40.) Just to the left of the border, one can expand in powers of the amplitude to obtain what is variously called a "Stokes" series (after Stokes' 1847 amplitude series for water waves) or a "Poincaré-Lindstedt" expansion. Whatever the name, the amplitude increases rapidly as one moves leftward to smaller ν for fixed ϵ so that the Stokes series is accurate only very close to the curving right border of the parameter space.

At the bottom of the diagram, $\epsilon = 0$, the RMKdV equation collapses into the KdV equation, and the sech-squared spike is the whole solution, unaccompanied by an outer region of oscillations. It is a curious fact that the KdV equation also furnishes an approximation in the *opposite* limit that $\epsilon \to \infty$. The zeroth order approximation is the KdV cnoidal wave for the special case

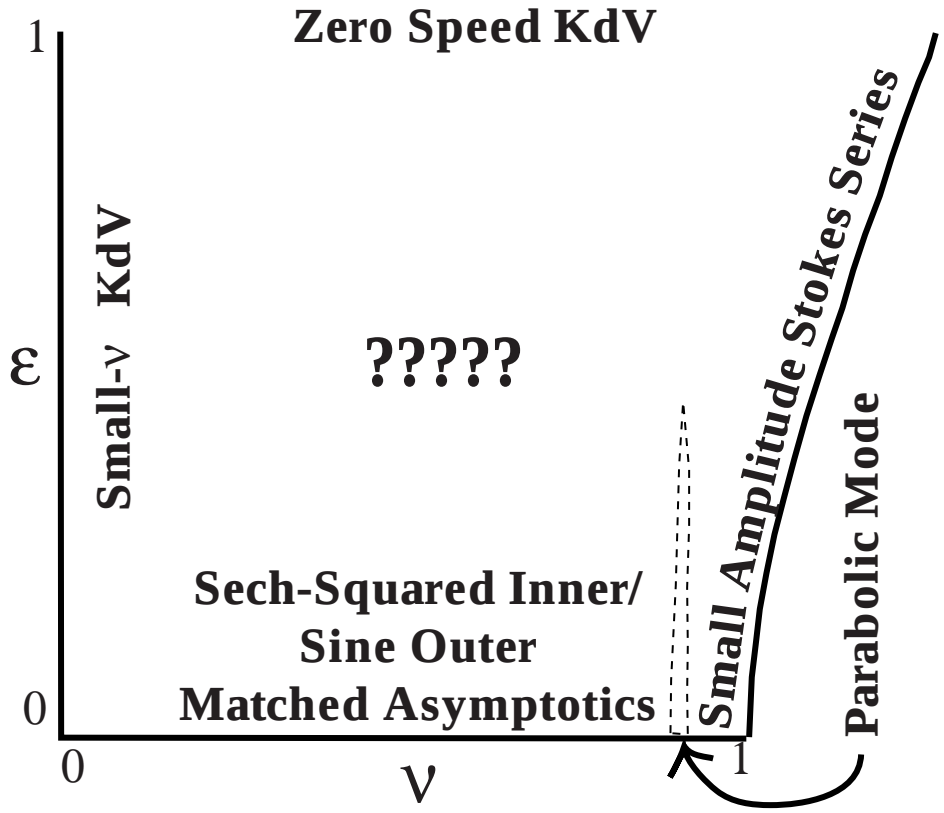

Fig. 1. Overview of the regime diagram. Quasi-cnoidal waves exist only when $0 \leq \nu \leq \nu_{max}(\epsilon) \equiv 2\epsilon/\sqrt{-2+2\sqrt{1+4\epsilon^2}}$, that is, to the left of the thick curve on the right. The question marks in the center denote the region where none of the analytic approximations is very accurate. The names of the analytic approximations label each of the four regimes where that approximation applies. The diagram does not show, because it is difficult to do so with clarity, that the analytic regimes have considerable overlap. The thin dotted region shows where three distinct shapes coexists with the first; we dub the shortest of these the "parabolic" mode because it is approximated by a parabola over most of the spatial period.

that the KdV speed is equal to zero. (For our purposes, the "KdV speed" is merely a mathematical abstraction, unrelated to the physical phase speed of the RMKdV quasi-cnoidal wave, which is always one in our convention.)

For small ν, the RMKdV equation can be approximated by the KdV cnoidal wave with a variable phase speed. For small ϵ, this approximation is quite accurate even for $\nu \approx 1/2$, thus strongly overlapping with the matched asymptotics region.

In the next four sections, we shall discuss each of the four analytic approximations in turn.

3 Matched Asymptotics for Small ϵ

This approximation was devised by Hunter[14] who obtained only the lowest order inner and outer approximations. We extended this to higher order[7,8]. Because the matched asymptotics expansion is derived in detail in our companion paper[8], we shall merely quote the result.

Define the auxiliary parameters

$$\Lambda_1 = 6\cot(\pi\,\nu); \qquad \Lambda_2 = 12\log(2) + 12 + \Lambda_1^2 \tag{5}$$

The composite expansion to $O(\epsilon^2)$ is

$$u \sim u^{(inner)} + u^{(outer)} - O_2 I_2 u \tag{6}$$

where each quantity on the right is defined below. This approximation is uniformly valid everywhere on the spatial period. It is convenient to introduce the abbreviations,

$$\sigma \equiv \mathrm{sech}(X/2); \qquad \tau \equiv \tanh(X/2); \qquad \Upsilon \equiv \log(\cosh(X/2)) \tag{7}$$

$$\mathcal{E} \equiv -1 + 3\sigma^2\,(1 - (X/2)\tau) \tag{8}$$

$$\Xi(X) \equiv \mathrm{dilog}\,(1/2 + \tau/2) \;-\; \mathrm{dilog}\,(1/2 - \tau/2) \tag{9}$$

where the dilogarithm function is as defined on pg. 1004 of [1]

$$\mathrm{dilog}(z) \equiv \;-\; \int_1^z \frac{\log(t)}{t-1}\,dt \tag{10}$$

The inner approximation is

$$\begin{aligned} u^{(inner)} = {} & 3\,\sigma^2 + \epsilon\Lambda_1\,\mathcal{E} \\ & + \epsilon^2\left\{12 - 12\tau^2 + 24\Upsilon - 36\tau^2\Upsilon - 9X\tau\sigma^2\Upsilon + (9\log(2) - 24)X\tau\sigma^2 + 9\tau\sigma^2\,\Xi\right\} \\ & + \epsilon^2\,\Lambda_2\,\mathcal{E} \\ & + \epsilon^2\,\Lambda_1^2\left\{-1 + \frac{3}{2}\tau^2 - \frac{3}{8}X(\tau + X/2)\sigma^2 + \frac{9}{16}X^2\tau^2\,\sigma^2\right\} \end{aligned} \tag{11}$$

The outer approximation is a Stokes series, that is, a Fourier series with coefficients in powers of the amplitude. To conform to Hunter[14], the phase speed c is fixed at one while the wavenumber k varies with ϵ; in other applications, it is more common to fix k and vary c. After collecting terms of equal ϵ order

and trigonometric factor, we have

$$a_1 = -\Lambda_1; \qquad b_1 = -6 \tag{12}$$

$$k \equiv 1 + \epsilon^2 \left\{ -\frac{1}{2} + \frac{1}{12} \left(a_1^2 + b_1^2 \right) \right\} \tag{13}$$

$$C_j \equiv \cos(j\, k\, \epsilon\, X), \qquad S_j \equiv \sin(j\, k\, \epsilon\, |X|), \qquad j = 1, 2 \tag{14}$$

$$\begin{aligned} u^{(outer)} = & \epsilon \left(a_1 C_1 + b_1 S_1 \right) \\ & + \epsilon^2 \left\{ \frac{1}{3}(a_1^2 - b_1^2) C_2 + \frac{2}{3} a_1 b_1 S_2 - \frac{5}{6} \Lambda_1^2 C_1 - 5 \Lambda_1 S_1 \right\} \end{aligned} \tag{15}$$

The second order outer limit of the second order inner approximation is

$$O_2 I_2(u) \equiv -\Lambda_1\, \epsilon - \epsilon^2 \left(12 + \frac{1}{2}\, \Lambda_1^2 \right) - 6 \epsilon^2 X \tag{16}$$

The complete second order solution is a bit of a mess, but the interpretation is not. In the inner region, u is a solitary wave of the KdV equation plus corrections at higher order in ϵ. In the outer region, the wave is a small amplitude sinusoidal oscillation plus small corrections in powers of the amplitude.

The coefficients of the expansion depend on the period parameter ν only through the parameter $\Lambda_1 = 6 \cot(\pi\nu)$. When $\nu = 1/2$ so that $\Lambda_1 = 0$, the first order inner correction is zero, the amplitude of the sinusoidal oscillations is minimized and the matched asymptotics expansion is most accurate for a given ϵ. As $\nu \to 0$ or $\nu \to 1$, the amplitude of the outer expansion tends to infinity and of course the perturbation expansion breaks down.

4 Large-ϵ Approximation: Zero-Speed KdV

4.1 Lowest Order Approximation

The analysis is simplified by defining a new spatial coordinate ζ such that period in ζ is always 2π:

$$\zeta \equiv \frac{\epsilon}{\nu} X \qquad \leftrightarrow X \equiv \zeta \frac{\nu}{\epsilon} \tag{17}$$

For large ϵ, the fourth derivative is too big to be balanced by any of the other terms in the equation except perhaps the nonlinear term, and then only if the amplitude is increasing as $O(\epsilon^2/\nu^2)$. This motivates the new unknown

$$u = \frac{\epsilon^2}{\nu^2}\, w(X;\epsilon) \tag{18}$$

which transforms the ODE to

$$(w_{\zeta\zeta\zeta} + w w_\zeta\,)_\zeta + \frac{1}{\epsilon^2}\left\{-\nu^2 w_{\zeta\zeta} - \nu^4\, w\right\} = 0 \qquad \text{[stationary RMKdV]} \tag{19}$$

In the limit $\epsilon \to \infty$ for fixed ν, the lowest order is now the KdV cnoidal wave of period 2π in ζ and zero phase speed which solves

$$W_{\zeta\zeta\zeta} + W W_\zeta = 0 \tag{20}$$

The formulas of Appendix D of [5] shows that

$$\begin{aligned} W(\zeta) &= -3.6481 + 10.9459 \sum_{m=-\infty}^{\infty} \mathrm{sech}^2\left\{\,0.9551\;(\zeta - 2\pi m)\right\} \\ &\approx 4.813\cos(\zeta) + 1.792\cos(2\zeta) + 0.518\cos(3\zeta) + 0.133\cos(4\zeta) + 0.032\cos(5\zeta) \end{aligned} \tag{21}$$

4.2 Corrections to the Zero-Speed KdV Approximation

At first order in $1/\epsilon^2$, the corrections are determined by numerically solving

$$\mathcal{L}^{(KdV)}\,\Omega_1 = W_{\zeta\zeta}, \qquad \mathcal{L}^{(KdV)}\,\Omega_2 = W \tag{22}$$

using a Fourier pseudospectral algorithm where

$$\mathcal{L}^{(KdV)} = \frac{d^4}{d\zeta^4} + W(\zeta)\frac{d^2}{d\zeta^2} + 2W_\zeta\frac{d}{d\zeta} + W_{\zeta\zeta} \tag{23}$$

The parameter-free solutions are (Fig. 2)

$$\Omega_1 \approx 2.334\cos(\zeta) + 1.617\cos(2\zeta) + 0.700\cos(3\zeta) + 0.240\cos(4\zeta) + 0.072\cos(5\zeta) \tag{24}$$

$$\Omega_2 \approx -1.816\cos(\zeta) - 1.601\cos(2\zeta) - 0.690\cos(3\zeta) - 0.2365\cos(4\zeta) - 0.071\cos(5\zeta) \tag{25}$$

It is interesting that the two are almost negatives of one another; the reason for this near-coincidence is not known.

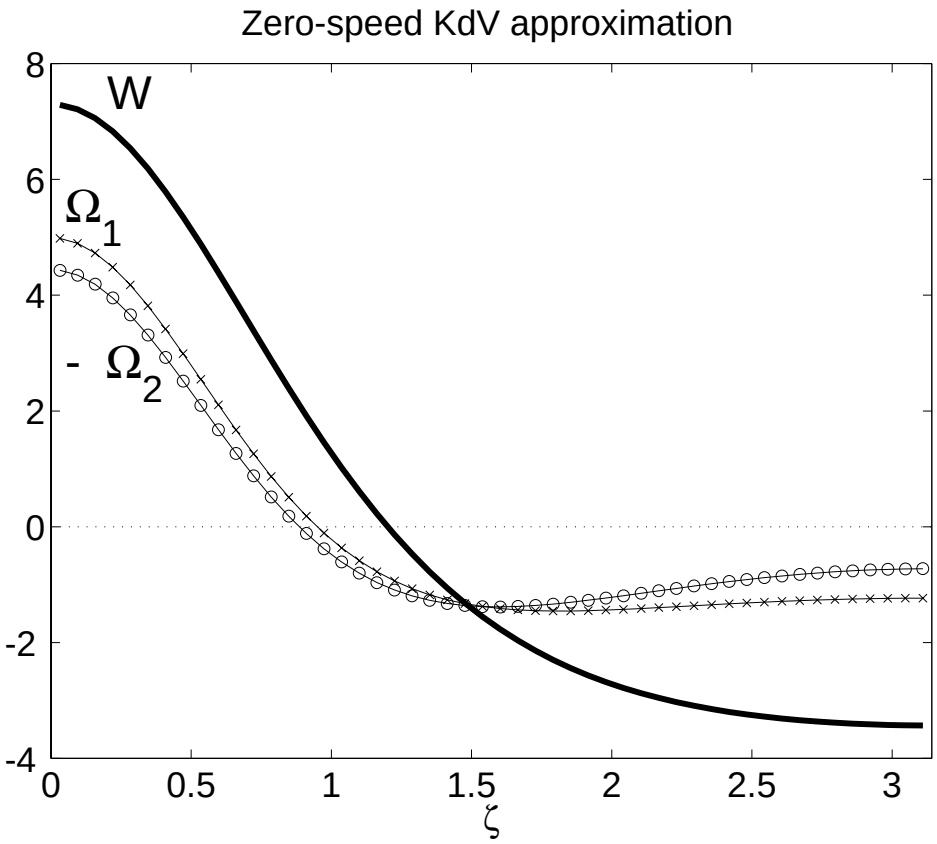

Fig. 2. Zero-speed KdV approximation for $\epsilon >> 1$ (very strong Coriolis). Thick solid curve: $W(\zeta)$, the lowest order approximation, which is the KdV cnoidal wave for the special case of a zero KdV phase speed. Line-with-x's: First order correction Ω_1. Line-with-circles: the NEGATIVE of Ω_2.

In terms of the original variables,

$$u \sim \frac{\epsilon^2}{\nu^2} W\left(\frac{\epsilon}{\nu} X\right) + \Omega_1\left(\frac{\epsilon}{\nu} X\right) + \nu^2 \Omega_2\left(\frac{\epsilon}{\nu} X\right) \tag{26}$$

5 Approximation for Small Spatial Period ($\nu << 1$): KdV Cnoidal Wave with Varying KdV Speed

Without approximation, the RMKdV equation with the same scalings as in the previous section is

$$(w_{\zeta\zeta\zeta} + w w_\zeta)_\zeta - \frac{\nu^2}{\epsilon^2} w_{\zeta\zeta} - \frac{\nu^4}{\epsilon^2} w = 0 \tag{27}$$

In the previous section, we took the limit $\epsilon \to \infty$ for fixed ν, which justifies neglecting the two rightmost terms. In this section, we shall instead assume

$$\nu^2 << \epsilon \tag{28}$$

and neglect only the rightmost term in the ODE to obtain the KdV equation:

$$(w_{\zeta\zeta\zeta} + w w_\zeta)_\zeta - \frac{\nu^2}{\epsilon^2} w_{\zeta\zeta} = 0 \tag{29}$$

The solutions are periodic with period 2π, as in the previous section, but the effective "phase speed" is

$$c_{KdV} \equiv \frac{\nu^2}{\epsilon^2} \tag{30}$$

Note that this is not the rate of travel of the RMKdV wave, which is always fixed at one in our convention, but rather the phase speed of the KdV cnoidal wave which gives an approximation to the RMKdV solution.

This "small-ν variable-speed KdV" approximation includes the zero-speed KdV approximation as a special case, the limit $\nu \to 0$ for fixed ϵ. It follows that the variable-speed approximation gives something new only for intermediate spatial period such that

$$\epsilon \sim> \nu << \sqrt{\epsilon}, \qquad \epsilon << 1 \tag{31}$$

The variable-speed KdV approximation is an elliptic function, which sounds alarming; however, the exact solution to the approximate ODE Eq. 29 is

$$w = -\frac{12}{\pi} B + 12 B^2 \sum_{m=-\infty}^{\infty} \mathrm{sech}^2(B[\zeta - 2\pi m]) \tag{32}$$

The crucial issue is how to compute the pseudowavenumber B.

Appendix D of [5] (where B is denoted by ϵ) shows that without approximation

$$\frac{\nu^2}{\epsilon^2} = -\frac{12}{\pi} B + 4B^2 - 24 B^2 \sum_{n=1}^{\infty} \mathrm{cosech}^2(2n\pi B) \tag{33}$$

As the KdV phase speed increases, B increases and the solitary wave becomes narrower. The worst case is $\epsilon \to \infty$ in the sense that B is smallest and the KdV solution is least soliton-like for this case. Even for this least favorable case, however, neglecting the infinite series gives an error in B of only 0.03%. It follows that it is a good approximation over the whole regime of interest — the whole regime where $c_{KdV} \geq 0$ — to approximate this transcendental equation by the quadratic equation

$$4\,B^2 \;-\; \frac{12}{\pi}\,B \;-\; \frac{\nu^2}{\epsilon^2} = 0 \tag{34}$$

The only root which is positive is

$$B = \frac{3}{\pi}\,\left\{\frac{1}{2} + \frac{1}{2}\sqrt{1 + \frac{\pi^2}{9}\,\frac{\nu^2}{\epsilon^2}}\;\right\} \tag{35}$$

Using the relationships $u = (\epsilon^2/\nu^2)w$ and $\zeta \equiv (\epsilon/\nu)\,X$, the KdV approximation to the RMKdV solution can be written

$$u = -\frac{12}{\pi}\frac{\epsilon^2}{\nu^2}\,B + 12B^2\,\frac{\epsilon^2}{\nu^2}\sum_{m=-\infty}^{\infty}\mathrm{sech}^2\left(B\frac{\epsilon}{\nu}\left[X - 2\pi m\frac{\nu}{\epsilon}\right]\right) \tag{36}$$

For small ϵ/ν, this can be simplified by using $B \approx (1/2)(\nu/\epsilon)$, which gives

$$u \approx -\frac{6}{\pi}\frac{\epsilon}{\nu} + 3\sum_{m=-\infty}^{\infty}\mathrm{sech}^2\left(\frac{1}{2}\left[X - 2\pi m\frac{\nu}{\epsilon}\right]\right), \qquad \text{Small}\,\epsilon \tag{37}$$

In this regime, the KdV approximation just gives the sech-squared spike of Hunter's matched asymptotic approximation. Thus, the variable-phase-speed-KdV approximation has a much wider range of usefulness in ϵ than the KdV-zero-speed approximation, which is accurate only for very large ϵ.

6 Stokes (Poincaré-Lindstedt) Expansion

When the period parameter ν is near $\nu_{max}(\epsilon)$, defined by Eq. 4 above, then the amplitude of the quasi-cnoidal wave is small. This makes it possible to expand the solution in powers of the amplitude. There is some freedom in the choice of "amplitude" parameter: ours is the coefficient a of the lowest harmonic, $\cos((\epsilon/\nu)X)$.

There is one technical complication. It is usual to expand the phase speed as a function of a while the spatial period is fixed. However, our convention is to

fix the phase speed c at one. This requires us to expand the wavenumber k:

$$k \equiv \frac{2\pi}{P} = \frac{\epsilon}{\nu} \approx k_0 + k_2 a^2 + k_4 a^4 + \ldots \tag{38}$$

If a is specified, then the equation above gives the corresponding spatial period. If the period is specified, then the equation $k(a) = \epsilon/\nu$ must be inverted to compute $a(\epsilon, \nu)$.

We shall restrict ourselves to the expansion up through and including $O(a^4)$, which allows $k(a)$ to be inverted by solving a quadratic equation in the unknown a^2:

$$a = \sqrt{-\frac{k_2}{2k_4} \pm \frac{1}{2k_4}\sqrt{(k_2^2 - 4k_4k_0 + 4k_4\frac{\epsilon}{\nu})}} \tag{39}$$

$$k_0 = \frac{1}{2}\sqrt{-2 + 2\sqrt{1+4\epsilon^2}} = \frac{\epsilon}{\nu_{max}(\epsilon)} \tag{40}$$

$$k_2 = \frac{1}{12}\,\frac{k_0^3}{4\,k_0^2 - 3\,\epsilon^2 + 10\,\epsilon^2\,k_0^2} \tag{41}$$

$$\begin{aligned} k_4 = \frac{1}{32}k_0^5(&-1146k_0^6\epsilon^2 + 10k_0^2\epsilon^4 + 7128k_0^8 + 540k_0^4 - 183\epsilon^2k_0^2 \\ &-1081\epsilon^2k_0^4 + 4356k_0^6 + 7\epsilon^4 - 864k_0^{10}) \\ /\ &((\epsilon^2 - 4k_0^2 - 16k_0^4)^3\,(2k_0^2+1)^3\,(\epsilon^2 - 9k_0^2 - 81k_0^4)) \end{aligned} \tag{42}$$

The Stokes expansion up to $O(\epsilon^4)$ is

$$u \approx a\cos(\zeta) + \left\{a^2a_{22} + a^4a_{24}\right\}\cos(2\zeta) + a^3a_{33}\cos(3\zeta) + a^4a_{44}\cos(4\zeta) \tag{43}$$

$$a_{22} = \frac{k_0^2}{15\,\epsilon^2 - 12\,k_0^2} \tag{44}$$

$$a_{33} = \frac{3}{16}\,\frac{k_0^2 - \epsilon^2}{36\,k_0^2 - 36\,\epsilon^2 + 85\,\epsilon^2\,k_0^2 - 50\,\epsilon^4} \tag{45}$$

$$a_{44} = 4k_0^2\,\frac{2a_{33} + a_{22}^2}{255\epsilon^2\ -\ 240\,k_0^2} \tag{46}$$

$$a_{24} = -2k_0\frac{4k_2a_{22} - k_2 - k_0a_{33} + 32\,k_0^2\,k_2a_{22}}{15\epsilon^2 - 12k_0^2} \tag{47}$$

7 Low Order Fourier Galerkin Approximation

Fourier spectral methods are usually regarded as numerical tools for solving differential equations; indeed, we used a high order Fourier pseudospectral method[5,6] to compute the "exact" solutions that are compared with various approximations below. However, at low order (one to three terms), spectral methods are often very successful in generating a simple but accurate analytical solution [9,2,6]. Most are linear; what is remarkable here is that the symbolic manipulation language Maple is able to produce explicit analytic solutions for up to three Fourier terms even though the differential equation is quadratically *nonlinear*. The entire Maple program is given as Table 1.

The numerical comparisons below show that the three-term Fourier-Galerkin approximation is just as accurate as the four-term Stokes approximation for $\nu \approx \nu_{max}(\epsilon)$. This is not surprising because the Stokes series shows that in this small amplitude regime, the quasi-cnoidal wave can be accurately approximated by a handful of Fourier components. What is surprising is that the Galerkin approximation is also accurate over the full range of ν so long as ϵ is sufficiently large. The reason is that the large-ϵ limit, which can be approximated by the KdV cnoidal wave of zero speed, is also the sum of a handful of Fourier terms as shown explicitly in Eq. 21.

Table 1
Fourier-Galerkin Maple program

```
k:=epsilon / nu;
u:=a1*cos(zeta) + a2*cos(2*zeta) + a3*cos(3*zeta);
Residual:=k**4*diff(u,zeta,zeta,zeta,zeta)
     +k*k* (u-1)*diff(u,zeta,zeta) + k*k*diff(u,zeta)*diff(u,zeta) - epsilon**2 *u;
Resid:=combine(Residual,trig); # Products of trig functions → Fourier series
eq1:=int(cos(zeta)*Resid,zeta=0..Pi);
eq2:=int(cos(2*zeta)*Resid,zeta=0..Pi);
eq3:=int(cos(3*zeta)*Resid,zeta=0..Pi);
asol:=solve({eq1,eq2,eq3},{a1,a2,a3});
```

Define the auxiliary variables

$$D_1 \equiv -\nu^4 + 9\nu^2\,(1+a_2) + 81\epsilon^2$$
$$D_2 \equiv \nu^8 - 13\nu^6 + 36\nu^4 + (-97\nu^4 + 468\nu^2)\epsilon^2 + 1296\epsilon^4 \tag{48}$$

The Fourier coefficients can be written as

$$
\begin{aligned}
a_2 &= -1 - 9\frac{\epsilon^2}{\nu^2} + \frac{1}{9}\nu^2 - \frac{1}{9}\sqrt{37\nu^4 - 378\nu^2 + 405 + 4698\frac{\epsilon^2}{\nu^2} + 9477\frac{\epsilon^4}{\nu^4} - 3114\epsilon^2} \\
a_1 &= \sqrt{a_2}\frac{\sqrt{D_2}}{\nu\sqrt{D_1}} \\
a_3 &= \frac{9}{2}\nu\,(a_2)^{3/2}\,\frac{\sqrt{D_2}}{\sqrt{D_1}\,(-\nu^4 + 9\nu^2 + 81\epsilon^2)}
\end{aligned}
\tag{49}
$$

The coefficients are out of the usual numerical order because a_2 must be evaluated before the others.

8 Piecewise-Parabola Approximation

It has long been known that the RMKdV equation has an exact solution in the form of a parabola[10,13,11,12]:

$$
u_{parab} = \frac{\epsilon^2}{6}X^2 + b\epsilon\,X + \left\{-\frac{1}{2} + \frac{3}{2}\,b^2\right\} \tag{50}
$$

where b is a free parameter. The parabola is unbounded, but if it is converted into a piecewise parabolic function, then the sum will be a bounded solution everywhere except at the points where the pieces join with discontinuous slopes. As noted earlier[10,13,8], the average of a solution over the spatial period must be zero. This constraint requires that the free parameter $b = -1$ and also that the period parameter $\nu = 3/\pi$, or in other words that the spatial period is $P = 6/\epsilon$. The parabola then generates the periodized, zero mean function

$$
\mathcal{P} \equiv u_{parab}(X - m(X)[6/\epsilon]) \tag{51}
$$

where $m(X)$ is an integer chosen so that

$$
X - m(X)\,(6/\epsilon)\ \in [0, 6/\epsilon] \tag{52}
$$

The shape and maximum amplitude are independent of ϵ, which controls only the spatial scale. Fig. 3 illustrates this function.

In the vicinity of the peaks where the slope is discontinuous, the approximation of u by the periodized parabola must fail. However, it is possible that the breakdown merely smooths the points of the periodized parabola in a narrow region without dramatically altering the solution elsewhere.

Earlier work[10,13] describes one such scenario: the inner approximation is

the solitary wave of the Korteweg-deVries equation and the outer approximation is the parabola. This branch of quasi-cnoidal waves has a maximum of three. In the limit of small ϵ, this approximation is identical (to within $O(\epsilon^4)$) with Hunter's first order approximation for the same spatial period. (Note that when there is less than one wavelength between peaks, the sine function which is Hunter's first order outer approximation is well-approximated by the parabola and vice versa.) The inner approximation is a spike that rises to three times the height of the parabola, which has a maximum of only one.

However, our numerical solutions show that there is also a second mode in which the peaks are smoothed far less dramatically without a spike as illustrated by Fig. 4. Only the crest is shown because for $\epsilon = 1/100$, the periodized-parabola and the smooth, continuous exact solution are graphically indistinguishable when plotted so as to show the entire spatial period.

This parabola-like shape is observed only in a small neighborhood of $\nu \approx 3/\pi$. We shall therefore let the numerical solutions speak for themselves.

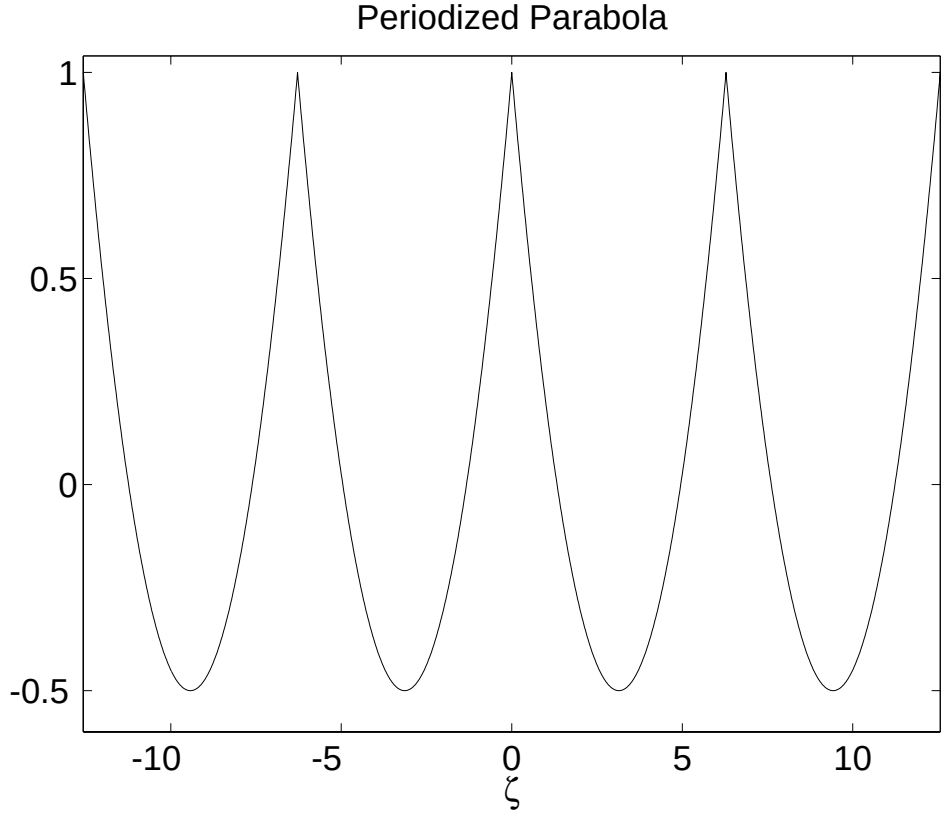

Fig. 3. The piecewise-parabola which is a solution of the RMKdV equation everywhere except at the joins ($\zeta = 0, \pm 2\pi, \pm 4\pi, \dots$).

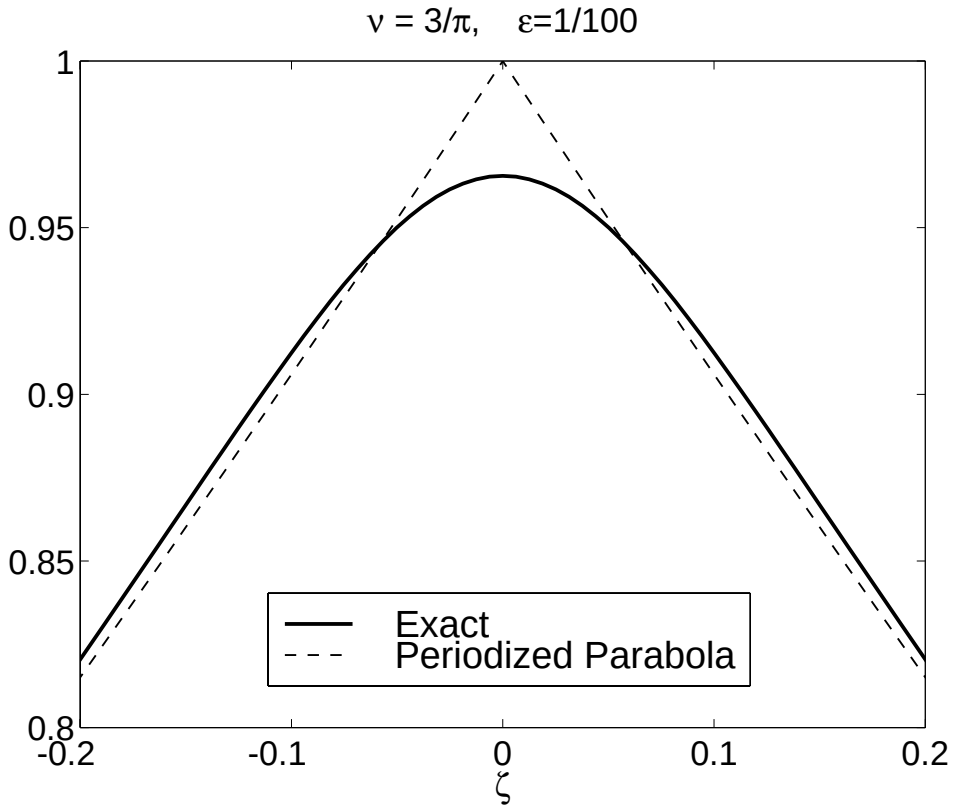

Fig. 4. A comparison of the exact quasi-cnoidal solution [thick solid curve] with the periodized parabola [dashed]. Note that this is a "zoom" plot which shows only a small PART of the FULL range in amplitude, $u \in [-0.501, 0.965]$, and only PART of a spatial period, which is $\zeta \in [-\pi, \pi]$.

9 Shapes of the Cnoidal Wave

9.1 Large ϵ

Fig. 5 shows u for various ν at $\epsilon = 1$. The spatial coordinate $\zeta \equiv \frac{\epsilon}{\nu} X$ is convenient for the graph because the spatial period is scaled to 2π for all ν and ϵ. For this and for all larger ϵ, the KdV-zero speed approximation is quite accurate except very close to $\nu = \nu_{max}(\epsilon)$. In this parametric boundary layer where $\nu_{max} - \nu << 1$, the amplitude decreases rapidly as ν_{max} is approached, and the 4-term Stokes series and 3-term Galerkin approximation both become very accurate.

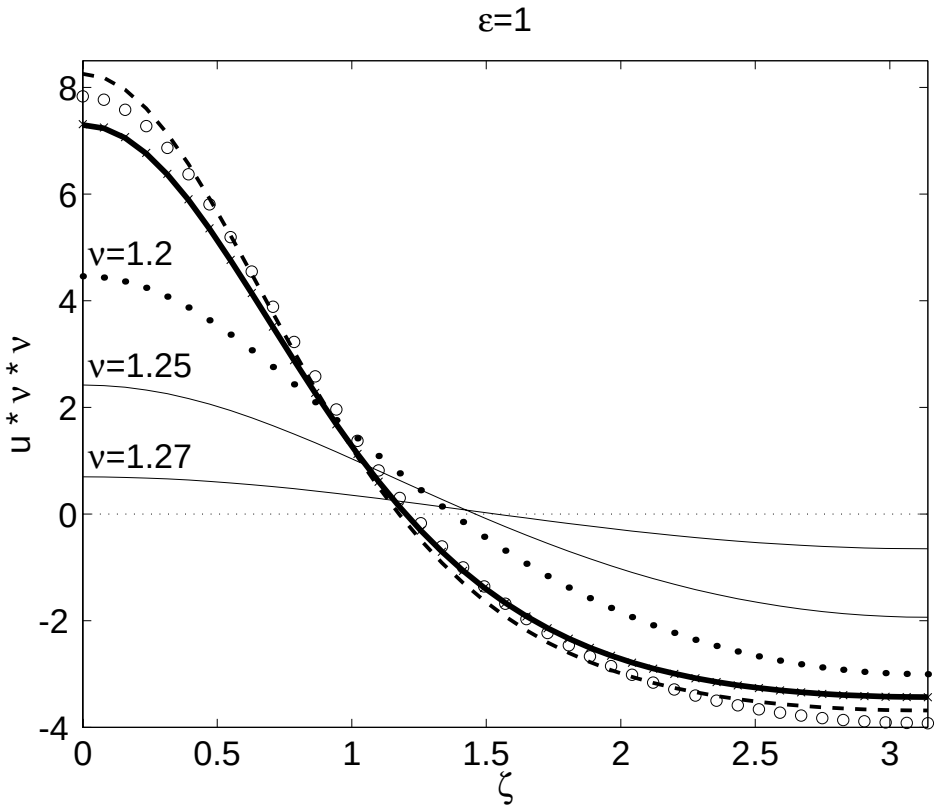

Fig. 5. $\epsilon = 1$. The unknown u is scaled by multiplication by ν^2. The three labelled curves are values of ν close to $\nu_{max}(1) = 1.271$. The amplitude decreases rapidly as ν_{max} is approached and the Stokes series becomes more and more accurate. The thick solid line is the KdV-zero speed cnoidal wave, which is the lowest order approximation in the limit $\epsilon \to \infty$. The three unlabelled curves are almost indistinguishable from the KdV cnoidal wave. x's: $\nu = 1/20$. Dashed: $\nu = 1/2$. Circles: $\nu = 0.999$.

9.2 Moderate ϵ

Fig. 6 is similar to the previous graph except that ϵ has been reduced by a factor of ten to $\epsilon = 1/10$. For both small ν (left panel) and large ν (right panel), the peak fills half or almost half of the interval. As noted earlier, the small ν regime is well-approximated by the KdV cnoidal wave; $\nu \approx 1$ is well-approximated by a Stokes (Poincaré-Lindstedt) expansion in small powers of the amplitude. In contrast, for intermediate ν, the wave has a narrow central peak and the matched asymptotics approximation is accurate. The inner/outer region decomposition of the matched asymptotics method does not give a good approximation for either small ν or ν near one because the inner region has expanded to fill the whole period, squeezing out the outer region.

Figs. 7 shows the contours of the wave over the whole range $\nu \in [0, \nu_{max}(\epsilon)]$. (When ϵ is small, ν_{max} is only slightly larger than one.) As in the previous graph, $\epsilon = 1/10$. The contours are squeezed close together at the bottom of the plot (small ζ, intermediate ν) where the peak at $\zeta = X = 0$ is well-approximated by $u \sim 3\mathrm{sech}^2(X/2)$, which is the solitary wave of the Korteweg-deVries equation.

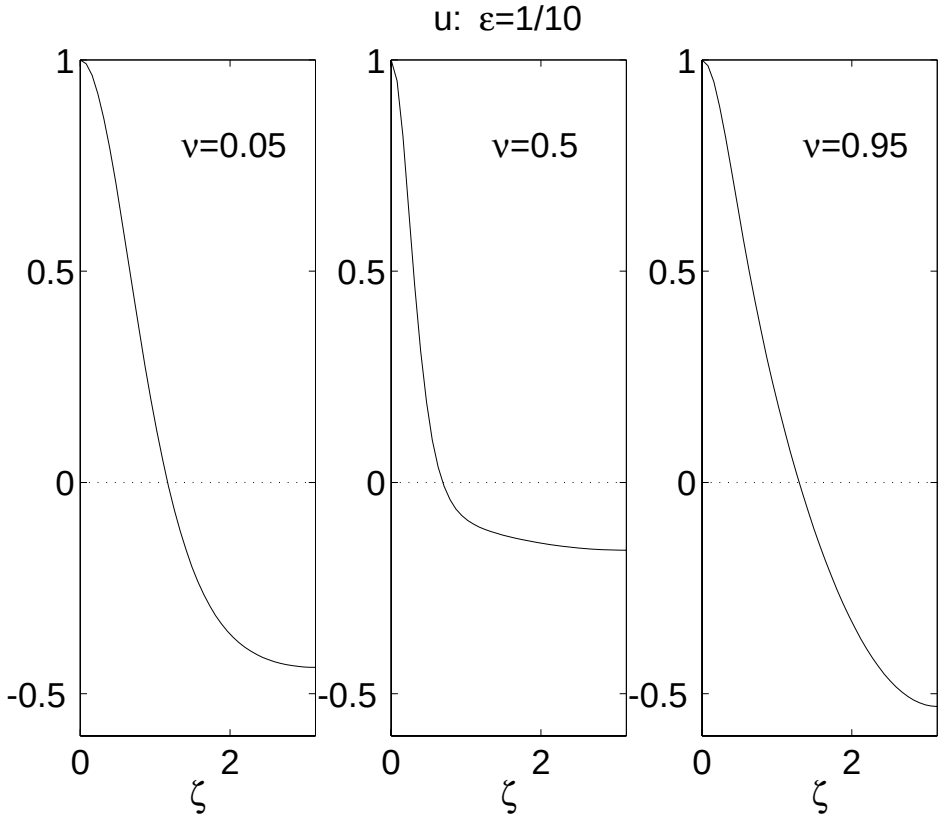

Fig. 6. Quasi-cnoidal wave u for $\epsilon = 1/10$ and for three different ν. Each plot has been scaled by dividing by the maximum of u for a given ν so that each graph has a maximum of one. The actual maxima of u are $\max(u) \sim O(12\,\epsilon^2/\nu^2)$ for small ν (left panel), which is very large; $\max(u) \approx 3$ for intermediate ν where the matched asymptotics approximation applies (middle graph); and $\max(u) << 1$ for $\nu \approx 1$ where the Stokes amplitude expansion is good (right panel).

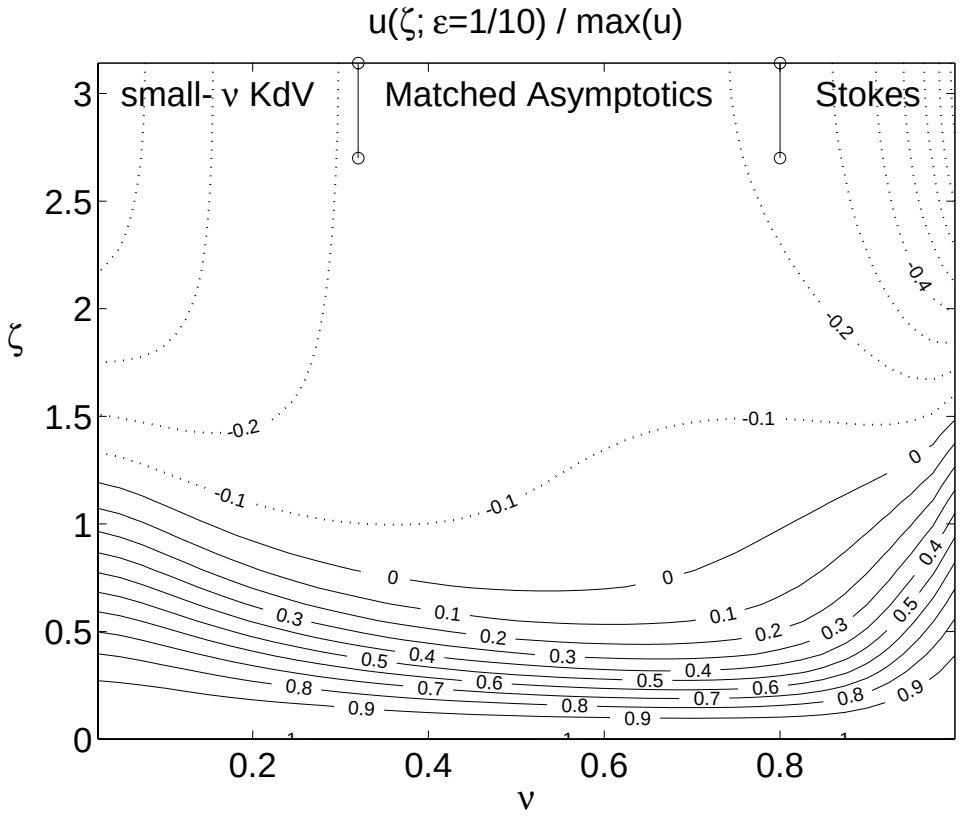

Fig. 7. $\epsilon = 1/10$, contours of $u(\zeta; \nu, \epsilon)$ at intervals of 1/10, scaled by dividing by the maximum of u for a given ν. Positive-valued contours are solid; isolines where $u < 0$ are dashed. The three approximations which apply and the rough boundaries of their domains are labeled at the top of the figure.

9.3 Small ϵ

The case of small ϵ is largely an exaggeration of moderate ϵ. The matched asymptotic approximation is valid over a larger and larger range in ν as ϵ decreases. Because the width of the $3\text{sech}^2(X/2)$ spike is fixed whereas the scale of the small amplitude, sinusoidal outer solution is widening inversely with ϵ, the spike becomes narrower and narrower compared to the spatial period.

The one new complication is that in the vicinity of $\nu \approx 3/\pi \approx 0.95493$, there are three different quasi-cnoidal shapes as illustrated for $\epsilon = 1/100$ in Fig. 8. The tallest is similar to that for smaller ν with a narrow spike rising from a sinusoidal background. The shortest shape, which is found only in the vicinity of $\nu \approx 3/\pi$, is well-approximated by the "periodized parabola" described in Sec. 8. The third solution is intermediate in both shape and amplitude between these two extremes.

We carefully describe these as different "shapes" because plotting the maximum of u versus ν and ϵ shows that these different shapes are part of a single continuous function. The surface $\max(u)(\nu, \epsilon)$ has a fold so that it is triple-valued in a small neighborhood of $\nu \approx 3/\pi$ for small ϵ. We have not attempted to accurately calculate the triple point where the fold begins, but it is around $\epsilon = 1/70, \nu = 3/\pi$.

The folded-over region is very narrow and thus perhaps not too important. Nevertheless, it illustrates the complexity hidden within a seemingly innocuous ordinary differential equation.

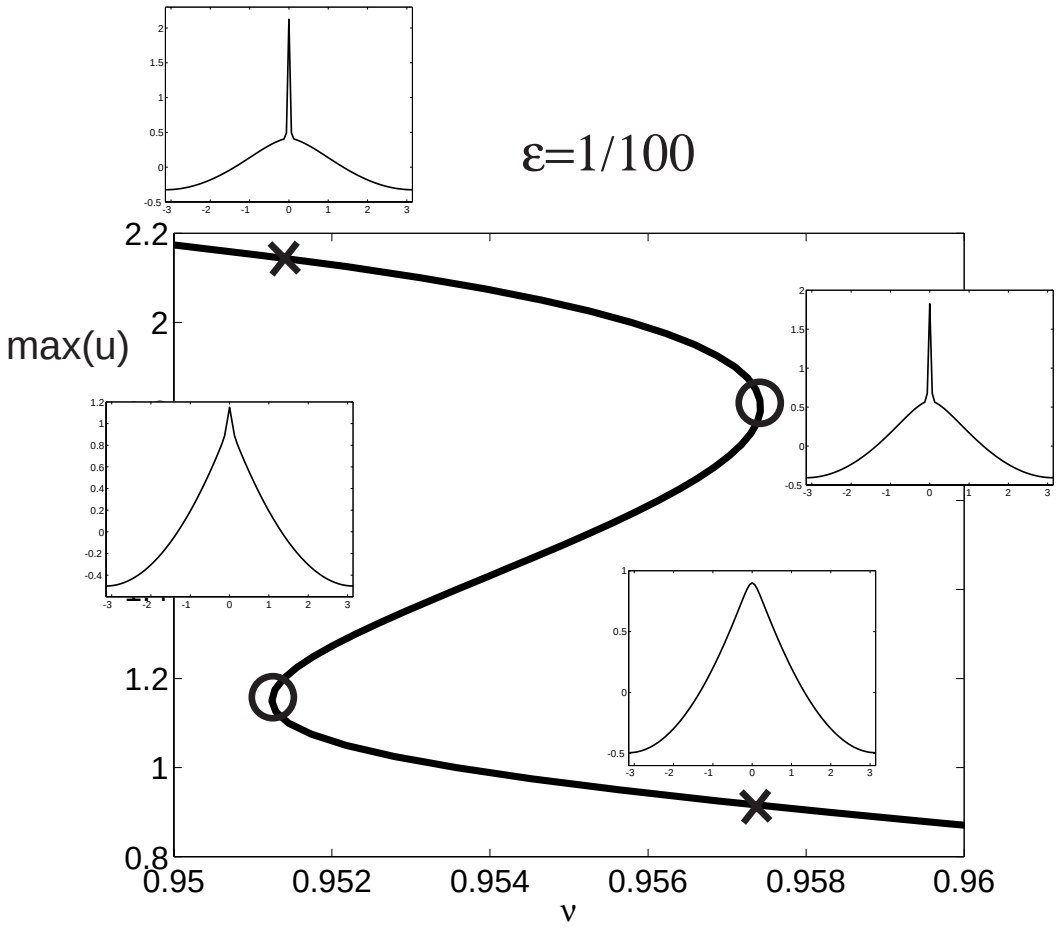

Fig. 8. The very thick, S-shaped curve is $\max_\zeta(u(\zeta;\epsilon,\nu))$ versus ν for $\epsilon = 1/100$. There are two limit points (marked by hollow circles) where the maximum develops a vertical slope; between them for $\nu \in [0.951, 0.957]$, there are two different modes. The four insets show the shape of $u(\zeta)$ at the two limit points and also the other mode that coexists at the same value of ν. (The x's mark the nonsingular points on the curve of $\max(u)$ where the third and fourth inset graphs are evaluated.)

10 Errors in the Approximations

Fig. 9 illustrates the errors in the approximations derived in earlier sections. Here, "error" is the maximum pointwise error, scaled by dividing by the maximum of u. Only contours where $\log_{10}$ error is a negative integer are shown; besides being contours of the error, the isolines collectively shade the regions where the relative error for a given approximation is less than 10%. The approximations almost fill the entire parameter space. One gap is a small region around $\nu \approx 3/\pi$ and small ϵ where the quasi-cnoidal wave folds upon itself so that three distinct modes coexist at each point of the $\nu - \epsilon$ within this region. The other gap is a small region for ν slightly larger than $1/2$ and moderate ϵ.

The zero speed KdV approximation is accurate down to rather surprisingly small ϵ — $1/3$ or less for all ν when the first order corrections are added. This is rather amazing given that it is an expansion in inverse powers of ϵ, and therefore expected to be accurate only when $\epsilon >> 1$.

The three-term Fourier Galerkin approximation is accurate for ν near $\nu_{max}(\epsilon)$ where the Stokes series is also successful. However, the low order Galerkin approximation is fairly effective for large ϵ, too. The reason is that the zero speed KdV cnoidal wave is rather accurately approximated by its first three harmonics.

The small-ν approximation is also surprisingly good: even for ν as large as $1/2$, this approximation in terms of the KdV cnoidal wave is accurate for all ϵ.

The matched asymptotics expansion of Hunter and the authors is accurate only in a rather small region of small ϵ and intermediate ν. It would seem, therefore, to be the least useful of the approximations described in the paper. The reality is just the opposite. In applications, the small ϵ regime is the interesting one. This is precisely where the matched asymptotics expansion shines for a region that widens and widens in ν as the effects of Coriolis force on the gravity wave become weaker and weaker (decreasing ϵ).

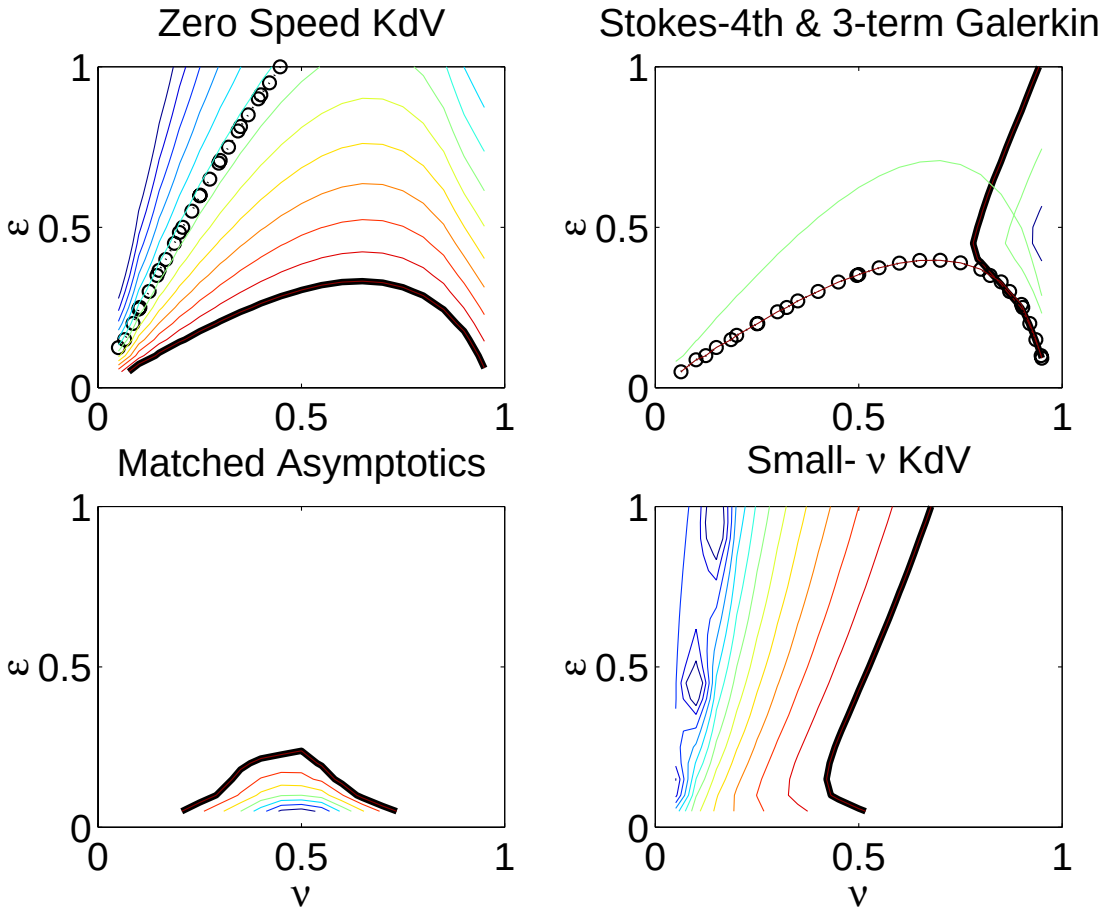

Fig. 9. The figure illustrates the contours of the logarithm (base 10) of the maximum pointwise (L_∞) error, scaled by $\max|u|$, for six different approximations. Only those contours where the relative error is less than 0.1 are shown; the boundary contours are drawn as thick lines or circles. Upper left: the thick lower curve below all others is the 10% relative error contour for the first order KdV-zero speed (large ϵ) approximation; the circles mark the same for the zeroth order approximation. Upper right: the thick solid curve is the 0.1 error contour for the 4-term Stokes amplitude series, which is accurate only to the right of the thick curve. The circles denote the 10% relative error for the 3-term Galerkin approximation. This is accurate for all large ϵ as well as where the Stokes series is satisfactory. The lower left shows the error contours for matched asymptotics. The lower right shows that the small-ν approximation is accurate even for ν as large as 1/2.

11 Multi-Initialized Newton/Fourier Numerical Algorithm

Our "exact" solutions were generated by first discretizing the RMKdV ODE using the Fourier pseudospectral method and then solving the resulting algebraic equations for the Fourier coefficients by means of Newton's iteration. The mechanics are thoroughly described in [5,3]. Analytical approximations, even with an accuracy of only 10% or less, are very effective for initializing Newton's iteration.

Unfortunately, there is no single analytical approximation that applies over the whole of the parameter space. We therefore adopted a "multi-initialization" strategy. Newton's iteration was applied several times, each with a different initialization, until either the iteration converged to within a given tolerance or until a preset number of iterations was exceeded. The ratio of the initial to the final residual was calculated for each sequence of iterates. The nonconvergent cases have final residuals only a little smaller than the initial residuals; the iterates from a "good" initialization had a huge ratio of initial to final residual, usually limited only by roundoff error. The iteration with the largest ratio was, if this ratio was large, accepted as the answer.

This multi-initialization strategy was not completely successful. It failed for $\nu \approx 3/\pi$ and small ϵ where the quasi-cnoidal wave has folded over to become three distinct shapes rather than one. It also sometimes failed for intermediate ϵ and moderate ν by converging to a mode with both large and tall peaks on a spatial period. By adding "if" statements to force the Newton iteration method to use a particular initialization thus overriding the residual ratio test, in particular regions of the $\nu - \epsilon$ plane, we were able to write a subroutine that would return accurate Fourier coefficients for the quasi-cnoidal wave almost everywhere in parameter space.

12 Summary

We have shown that the steadily-travelling, spatially periodic solutions of the RMKdV wave have many different regimes, each described by a different approximation, even when we restrict attention to the waves that have crests that are all of the same size, the "quasi-cnoidal" waves. In a small region of parameter space, the mode folds upon itself so that are three distinct quasi-cnoidal waves for a given value of the rotation parameter and spatial period.

One open problem is to systematically derive a matched asymptotic approximations to the new mode found by the authors. This has an outer approximation that is a piecewise parabola and an inner solution which slightly rounds

the crests where the pieces of the parabola join. Numerical solutions show that the inner region is indeed small compared to the outer region with a ratio of length scales that seems to increase with decreasing ϵ, exactly as required for matched asymptotics.

Another open problem, which is pursued in our companion article[8], is to show how the more complicated travelling waves, which have a mixture of tall and short peaks, bifurcate from the quasi-cnoidal waves studied here.

This work was supported by National Science Foundation through OCE9521133. Dr. Chen is grateful for a three-year graduate fellowship provided by the Department of Education, Taiwan, R. O. C.

References

[1] M. Abramowitz and I. A. Stegun, Handbook of Mathematical Functions, Dover, New York (1965).

[2] J. P. Boyd, Chebyshev and Legendre spectral methods in algebraic manipulation languages, J. Symb. Comput., 16, 377–399 (1993).

[3] J. P. Boyd, Pseudospectral/Delves-Freeman computations of the radiation coefficient for weakly nonlocal solitary waves of the Third Order Nonlinear Schroedinger Equation and their relation to hyperasymptotic perturbation theory, J. Comput. Phys., 138, 665–694 (1997).

[4] J. P. Boyd, The Devil's Invention: Asymptotics, superasymptotics and hyperasymptotics, Acta Applicandae 56, 1–98 (1999).

[5] J. P. Boyd, Weakly Nonlocal Solitary Waves and Beyond-All-Orders Asymptotics: Generalized Solitons and Hyperasymptotic Perturbation Theory, vol. 442 of Mathematics and Its Applications, Kluwer, Amsterdam, (1998).

[6] J. P. Boyd, Chebyshev and Fourier Spectral Methods, Dover, New York, (2000).

[7] G.-Y. Chen, Application of Weak Nonlinearity in Ocean Waves, Ph. D. dissertation, University of Michigan, Department of Atmospheric, Oceanic and Space Science, (1998).

[8] G.-Y. Chen and J. P. Boyd, Analytical and numerical studies of weakly nonlocal solitary waves of the Rotation-Modified Korteweg-deVries equation, Physica D, submitted (2000).

[9] B. A. Finlayson, The Method of Weighted Residuals and Variational Principles, Academic, New York, (1973).

[10] O. A. Gilman, R. Grimshaw, and Y. A. Stepanyants, Approximate analytical and numerical solutions of the stationary Ostrovsky equation, Stud. Appl. Math., 95 , 115–126 (1995).

[11] O. A. Gilman and R. Grimshaw and Yu. A. Stepanyants, Dynamics of internal solitary waves in a rotating fluid, Dyn. Atmos. Oceans, 23, 403–411 (1996).

[12] R. H. J. Grimshaw and J.-M. Heand L. A. Ostrovsky, Terminal damping of a solitary wave due to radiation in rotational systems, Stud. Appl. Math., 101 , 197–210 (1998).

[13] R. Grimshaw, L. A. Ostrovsky, V. I. Shrira, and Y. A. Stepanyants, Nonlinear surface and internal gravity waves in a rotating ocean, Surveys in Geophysics, 19, 289–338 (1998).

[14] J. K. Hunter, Numerical solutions of some nonlinear dispersive wave equations, Lectures in Applied Mathematics, 26, pp. 301–316 (1990)